Available online at www.sciencedirect.com
SCIENCE DIRECT®
Journal of Solid State Chemistry 170 (2003) 320–329
JOURNAL OF SOLID STATE CHEMISTRY
http://elsevier.com/locate/jssc

High-pressure preparation, crystal structure, and properties of the new rare-earth oxoborate β-$Dy_2B_4O_9$

Hubert Huppertz,* Sandra Altmannshofer, and Gunter Heymann

Department Chemie, Ludwig-Maximilians-Universität München, Butenandtstraße 5-13 (Haus D), 81377 München, Germany

Received 30 July 2002; received in revised form 19 September 2002; accepted 24 September 2002

Abstract

In this work we report about a new rare-earth oxoborate β-$Dy_2B_4O_9$ synthesized under high-pressure/high-temperature conditions from Dy_2O_3 and boron oxide B_2O_3 in a B_2O_3/Na_2O_2 flux with a walker-type multianvil apparatus at 8 GPa and 1000°C. Single crystal X-ray structure determination of β-$Dy_2B_4O_9$ revealed: $P\bar{1}$, $a = 616.2(1)$ pm, $b = 642.8(1)$ pm, $c = 748.5(1)$ pm, $\alpha = 102.54(1)°$, $\beta = 97.08(1)°$, $\gamma = 102.45(1)°$, $Z = 2$, $R1 = 0.0151$, $wR_2 = 0.0475$ (all data). The compound exhibits a new structure type which is built up from bands of linked BO_3- (Δ) and tetrahedral BO_4-groups ($\square$). The Dy^{3+}-cations are positioned in the voids between the bands. According to the conception of fundamental building blocks β-$Dy_2B_4O_9$ can be classified with the notation $2\Delta6\square{:}\Delta\langle 3\square\rangle = \langle 4\square\rangle = \langle 3\square\rangle\Delta$. Furthermore we report about temperature-resolved in situ powder diffraction measurements and IR-spectroscopic investigations on β-$Dy_2B_4O_9$.

Keywords: High-pressure; Multianvil; β-$Dy_2B_4O_9$; Borates; Crystal structure

1. Introduction

Recent research in synthesis and characterization of new inorganic borates has focused on their interesting physical properties, which make them attractive for numerous practical applications as optical compounds, for instance, materials for second harmonic generation or host materials for fluorescence [1–3]. The rare-earth borates were synthesized starting from boron oxide B_2O_3 and the rare-earth oxides Ln_2O_3 whereby compound formation was observed for the molar ratios 1:1, 1:3, and 3:1 as shown below [4]:

$$B_2O_3 + Ln_2O_3 \rightarrow 2\ LnBO_3, \quad (1)$$

$$B_2O_3 + 3\ Ln_2O_3 \rightarrow 2\ Ln_3BO_6, \quad (2)$$

$$3\ B_2O_3 + Ln_2O_3 \rightarrow 2\ LnB_3O_6. \quad (3)$$

The rare-earth orthoborates $LnBO_3$ exhibit polymorphism, which led to a large number of studies concerning their crystallographic structures and chemical properties [5]. Recently, we were able to synthesize two new polymorphs χ-$DyBO_3$ and χ-$ErBO_3$, which contain layers built up from the new non-cyclic $[B_3O_9]^{9-}$-anions exhibiting one trigonal BO_3- (Δ) and two tetrahedral BO_4-groups ($\square$) according to $1\Delta2\square{:}\Delta2\square$ [6].

It has been known that rare-earth borates of the composition "Ln_3BO_6" crystallize in three different monoclinic structures [7] as Ln varies from La to Lu. Bartram determined the space groups of these compounds by Weissenberg techniques and refined the lattice constants from X-ray powder diffraction patterns [8]. The compounds were reported to crystallize in four different space groups, i.e., $P2_1/c$ for Ln = La to Nd and $C2/m$, $C2$, or Cm for Ln = Pm to Yb. The composition of these compounds was established by phase analysis only and was considered to be the most rare-earth cation-rich phase in the system Ln_2O_3–B_2O_3.

Recently, Lin et al. established the crystal structures of "La_3BO_6" [9], "Y_3BO_6" [10], and "Gd_3BO_6" [11] where they found that the compositions of these compounds are not as simple as those proposed previously. From the single-crystal structure analysis, the composition of the lanthanum compound was found to be $La_{26}(BO_3)_8O_{27}$, which shows a slight La_2O_3 excess relative to La_3BO_6 (8 $La_3BO_6 \cdot La_2O_3$). In contrast to these results, the yttrium compound $Y_{17.33}(BO_3)_4(B_2O_5)_2O_{16}$ and the gadolinium compound

*Corresponding author. Fax: +49-89-2180-7806.
E-mail address: huh@cup.uni-muenchen.de (H. Huppertz).

0022-4596/03/$ - see front matter © 2002 Elsevier Science (USA). All rights reserved.
doi:10.1016/S0022-4596(02)00099-3

$Gd_{17.33}(BO_3)_4(B_2O_5)_2O_{16}$, determined by X-ray powder diffraction data, were found to have an excess of borate. Although the Rietveld refinements resulted in fairly residual values, a couple of uncertainties remained.

LnB_3O_6 metaborates were obtained with Ln = Y, La, Ce, Pr, Nd by Canneri [12], with Ln = Pr to Tb (except Pm) by Tananaev et al. [13], with Ln = La to Tb by Bambauer et al. [14], and with Ln = Y, Dy to Lu by Tananaev et al. [15]. Recently, a new structure refinement on monoclinic $Pr(BO_2)_3$ was carried out by Sieke et al. [16].

All these oxoborates are characterized by a high structural flexibility caused in the linkage of planar/non-planar BO_3-groups and BO_4-tetrahedra, which can occur as isolated or condensed fundamental building blocks.

Searching for new compounds in the system Ln_2O_3–B_2O_3, we found that it is possible to realize the new compositions $Ln_4B_6O_{15}$ (Ln = Dy, Ho) [17, 18] and α-$Ln_2B_4O_9$ (Ln = Eu, Gd, Tb, Dy) [19][1] under extreme high-pressure/high-temperature conditions:

$$3\ B_2O_3 + 2\ Ln_2O_3 \xrightarrow{HP/HT} Ln_4B_6O_{15}, \quad (4)$$

$$2\ B_2O_3 + Ln_2O_3 \xrightarrow{HP/HT} \alpha - Ln_2B_4O_9. \quad (5)$$

In contrast to all nearly 500 structurally characterized oxoborates, wherein the linkage of BO_3- and BO_4-units occurs exclusively via corners, it can be pointed out that these oxoborates are the first examples exhibiting edge-sharing BO_4-tetrahedra next to corner-sharing BO_4-tetrahedra.

In this work, we report about our further attempts to explore for quaternary phases in the system Na–Dy–B–O under high-pressure/high-temperature conditions. In contrast to an expected quaternary phase, our synthesis resulted in a new polymorph β-$Dy_2B_4O_9$, whereby the added Na_2O_2 or Na_2CO_3 with a surplus of B_2O_3 acted as flux materials.

2. Experimental

According to the following equation, the new polymorph β-$Dy_2B_4O_9$ is synthesized from B_2O_3 (from H_3BO_3 (99.8%, Merck, Darmstadt) fired at 600°C) and the rare-earth oxide Dy_2O_3 (99.9%, Sigma-Aldrich, Taufkirchen) with additional Na_2O_2 and B_2O_3 as a flux.

$$2\ B_2O_3 + Dy_2O_3 \xrightarrow[8.0\,GPa,\ 1000°C]{Na_2O_2/B_2O_3\ Flux} \beta\text{-}Dy_2B_4O_9. \quad (6)$$

The exact molar ratio including the flux materials was B_2O_3:Dy_2O_3:Na_2O_2 = 3:1:1. All compounds were mixed thoroughly under air and loaded into a 3.66 mm outside diameter, 0.33 mm wall thickness, and 6.0 mm length hexagonal boron nitride cylinder that was sealed by a BN plate. The sample cylinder was placed in the center of a cylindrical resistance heater (graphite) that had a variable (stepped) wall thickness in order to minimize the thermal gradient along the sample [20–23]. MgO rods filled the space at the top and the bottom of the sample. A cylindrical zirconia sleeve surrounding the furnace provided thermal insulation. As pressure medium, Cr_2O_3-doped MgO octahedra (Ceramic Substrates & Components Ltd., Isle of Wight) with an edge length of 18 mm was used. A hole was drilled in the octahedron, the cylindrical assembly positioned inside and contacted with a molybdenum ring at the top and a molybdenum plate at the bottom. The experimental temperature was monitored using a $Pt/Pt_{87}Rh_{13}$ thermocouple that was inserted axially into the octahedral assembly with the hot junction in contact with the boron nitride cylinder. Eight tungsten carbide cubes separated by pyrophyllite gaskets (Plansee, Reutte, TSM10, edge length: 32 mm) with a truncation of 11 mm were used to compress the octahedron (“18/11 assembly” in conventional terminology) via a modified Walker-style split-cylinder multianvil apparatus [20]. For further details concerning the Walker-type module and multianvil experiments, see Refs. [21–23].

For the synthesis of β-$Dy_2B_4O_9$, the assembly was compressed in 3 h to 8 GPa and heated up to 1000°C in the following 10 min. After holding this temperature for 6 min, the sample was quenched by turning off the power with a quench rate of >500°C/s. After decompression the recovered experimental octahedron was broken apart and the sample carefully separated from the surrounding BN. The sample showed mainly colorless crystalline parts next to colorless amorphous areas. Investigations via EDX with a Jeol JFM-6500F (Analytical Field Emission Scanning Electron Microscope) clearly exhibited that in the crystalline parts, the elements dysprosium, boron, and oxygen were detectable, whereas in the amorphous regions also sodium was found next to dysprosium, boron, and oxygen. The separation of colorless single crystals of β-$Dy_2B_4O_9$ worked without any difficulties. Fig. 1 shows the powder diffraction pattern of the bulk material (Fig. 1a) in comparison to the simulated powder pattern of β-$Dy_2B_4O_9$ (Fig. 1b). Nearly all reflections of the measured pattern correspond to the simulation. Surplus Na_2O_2, the thermal decomposition product Na_2O ($Na_2O_2 \rightarrow Na_2O + 1/2\ O_2$), B_2O_3, or additional reaction products of these materials remain mainly in the amorphous state.

To investigate the reactions in the system B_2O_3/Dy_2O_3/Na_2O_2, we performed further experiments with

[1] H. Huppertz, unpublished results; the obtained diffraction pattern of α-$Dy_2B_4O_9$ was indexed on the basis of a monoclinic unit cell. The lattice parameters (a = 2520.2(4) pm, b = 440.6(1) pm, c = 2478.2(6) pm, β = 99.90(1)°) were obtained from least square fits of the powder data. α-$Dy_2B_4O_9$ is isotypic to α-$Ln_2B_4O_9$ (Ln = Eu, Gd, Tb) [19].

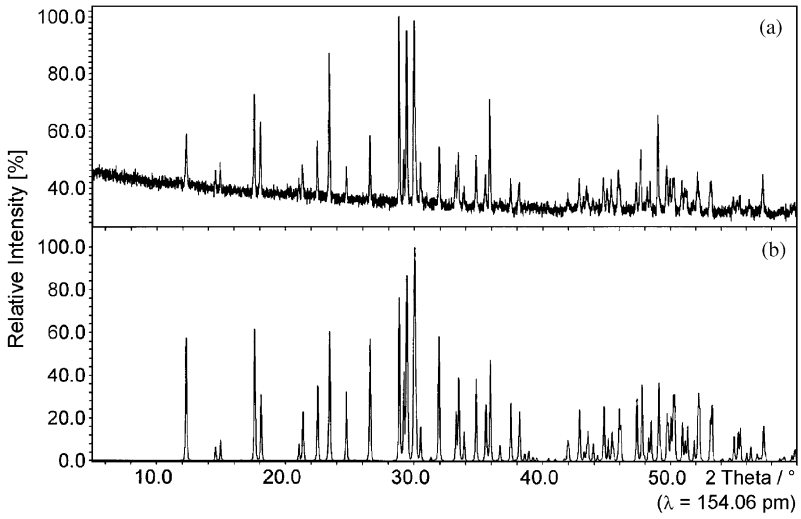

Fig. 1. Powder pattern of the bulk-material (a) (transmission geometry) and simulated powder pattern (b) of β-$Dy_2B_4O_9$. Deviations of the intensities result from texture effects.

Table 1
Results of the experiments in the system $B_2O_3/Dy_2O_3/Na_2O_2$ with various molar ratios. In the bottom part of the table Na_2O_2 was substituted by Na_2CO_3

B_2O_3	Dy_2O_3	Na_2O_2	Result
3	1	1	β-$Dy_2B_4O_9$
2	1	1	α-$Dy_2B_4O_9$
2	1	0	α-$Dy_2B_4O_9$
3	1	0	Mainly β-$Dy_2B_4O_9$
B_2O_3	Dy_2O_3	Na_2CO_3	Result
3	1	1	β-$Dy_2B_4O_9$

various molar ratios. Table 1 gives an overview of the molar ratios used under comparable high-pressure/high-temperature conditions. The best result for the successful synthesis of β-$Dy_2B_4O_9$ in the system $B_2O_3/Dy_2O_3/Na_2O_2$ was reached using a molar ratio of 3:1:1. Less B_2O_3 (2:1:1) or reactions without Na_2O_2 (2:1:0) resulted in the synthesis of α-$Dy_2B_4O_9$. Synthesis in a surplus of B_2O_3 without Na_2O_2 resulted mainly in β-$Dy_2B_4O_9$ with additional reflections of a second phase in the powder pattern. Apparently, the combination of surplus B_2O_3 with Na_2O_2 is the best flux-composition for the synthesis of β-$Dy_2B_4O_9$. It is also possible to substitute Na_2O_2 by Na_2CO_3 (Table 1, bottom). In contrast to the colorless reaction product using Na_2O_2, the usage of Na_2CO_3 leads to a black sample. A closer view with an optical microscope exhibits a mixture of colorless crystals (β-$Dy_2B_4O_9$) in combination with black powder. Evidently, the flux material is colored black by graphite from the decomposition of Na_2CO_3. At this point, we want to mention that until now nothing can be said about the composition or decomposition of the flux-material under these extreme high-pressure/high-temperature conditions.

In fact at normal pressure, there exist several sodium-rich borates like $NaBO_2$ [24], $Na_4B_2O_5$ [25], Na_3BO_3 [26] and also boron-rich phases like α-$Na_2O \cdot 3\ B_2O_3$ [27], β-$Na_2O \cdot 3\ B_2O_3$ [28], or $Na_2O \cdot 4\ B_2O_3$ [29] synthesized from the starting materials Na_2O and B_2O_3. Additionally, Mascetti et al. and Zhang et al. reported about rare-earth sodium borates $Na_3Ln(BO_3)_2$ (Ln = La, Nd [30]) (Ln = Y, Gd [31]). Nevertheless, there are several synthetic routes using mixtures of Na_2O/B_2O_3 as a flux material. For example, the synthesis of $M(BO_2)_3$ with M = Y, Dy to Lu is performed from a flux with the composition $Na_2O \cdot 19\ B_2O_3$ [15] without incorporating sodium into the reaction product.

3. Crystal structure analysis

The powder diffraction data of β-$Dy_2B_4O_9$ were collected on a STOE Stadi P powder diffractometer with monochromized Cu$K\alpha_1$ radiation. The obtained diffraction pattern was indexed with the program ITO [32] on the basis of a primitive unit cell. The lattice parameters (a = 617.0(1) pm, b = 643.4(1) pm, c = 749.0(1) pm, α = 102.56(1)°, β = 97.08(2)°, γ = 102.47(2)°, Table 2) were obtained from least-squares fits of the powder data. The correct indexing of the pattern was ensured by intensity calculations[2] taking the atomic positions from the structure refinements. The lattice parameters determined from the powder and the single crystal agreed well (Table 2).

Small single crystals were isolated by mechanical fragmentation and examined by Buerger precession photographs. Single-crystal intensity data were collected from a regularly shaped colorless crystal (block) at room

[2] $WinX^{POW}$ Software, STOE & CIE GmbH, Darmstadt, (1998).

Table 2
Crystal data and structure refinement for β-$Dy_2B_4O_9$

Empirical formula	β-$Dy_2B_4O_9$
Molar mass	512.24 g/mol
Crystal system	Triclinic
Space group	$P\bar{1}$ (No. 2)
Powder diffractometer	STOE Stadi P
Radiation	Cu$K\alpha_1$ ($\lambda = 154.06$ pm)
Unit-cell dimensions	$a = 617.0(1)$ pm
	$b = 643.4(1)$ pm
	$c = 749.0(1)$ pm
	$\alpha = 102.56(1)^\circ$
	$\beta = 97.08(2)^\circ$
	$\gamma = 102.47(2)^\circ$
Volume	0.278(1) nm^3
Diffractometer	Enraf-Nonius Kappa CCD
Radiation	Mo$K\alpha$ ($\lambda = 71.073$ pm)
Unit-cell dimensions	$a = 616.2(1)$ pm
	$b = 642.8(1)$ pm
	$c = 748.5(1)$ pm
	$\alpha = 102.54(1)^\circ$
	$\beta = 97.08(1)^\circ$
	$\gamma = 102.45(1)^\circ$
Formula units per cell	$Z = 2$
Calculated density	6.118 g/cm^3
Crystal size	$0.04 \times 0.05 \times 0.07$ mm^3
Detector distance	30.0 mm
Exposure time/degree	180 s
Absorption coefficient	26.7 mm^{-1}
$F(0\,0\,0)$	448
θ range	3.3–32.5°
Range in hkl	± 9, ± 9, ± 11
Scan type	φ/ω
Total no. of reflections	9591
Independent reflections	2015 ($R_{int} = 0.0335$)
Reflections with $I > 2\sigma(I)$	1961 ($R_{sigma} = 0.0304$)
Data/parameters	2015/137
Absorption correction	Numerical (HABITUS [33])
Transm. ratio (max/min)	1.52
Goodness-of-fit on F^2	1.230
Final R indices [$I > 2\sigma(I)$]	$R_1 = 0.0139$
	w$R_2 = 0.0384$
R indices (all data)	$R_1 = 0.0151$
	w$R_2 = 0.0475$
Extinction coefficient	0.0291(7)
Largest diff. peak and hole	1.29 and -1.21 e/Å^3

temperature by use of an Enraf-Nonius Kappa CCD equipped with a rotating anode (Mo$K\alpha$ radiation ($\lambda = 71.073$ pm)). A numerical absorption correction (HABITUS [33]) was applied to the data. All relevant information concerning the data collection are listed in Table 2. A systematic analysis of the dataset showed that no systematic extinctions were observed which is compatible with the space groups $P1$ and $P\bar{1}$. The centrosymmetric group was found to be correct during the structure refinement. The starting positional parameters were deduced from an automatic interpretation of direct methods with SHELXS-97 [34] and the structure was successfully refined with anisotropic atomic displacement parameters for all atoms using SHELXL-97 (full-matrix least-squares on F^2) [35]. Final difference Fourier syntheses revealed no significant residual peaks (see Table 2). Final positional and thermal displacement parameters together with the interatomic distances are listed in Tables 3–5. Listings of the observed/calculated structure factors and other details are available from the Fachinformationszentrum Karlsruhe, D-76344 Eggenstein-Leopoldshafen (Germany), e-mail: crysdata@fiz-karlsruhe.de, by quoting the registry number CSD-412659.

4. Results and discussion

The crystal structure of β-$Dy_2B_4O_9$ (Fig. 2) is built up from bands of linked BO_3-triangles and BO_4-tetrahedra. The bands run along [100] whereas the Dy^{3+}-cations are positioned in the voids between the bands. Fig. 3 gives a view of the crystal structure along [001]. Inside the bands the BO_4-tetrahedra (hatched polyhedra) form three membered rings which are quite common in borate crystal chemistry [36]. These B_3O_9-rings are linked to the next B_3O_9-ring via two trigonal BO_3-groups forming a six-membered ring (Fig. 4). Additionally, the B_3O_9-ring is connected to the next B_3O_9-unit via two common corners forming a four-membered ring (Fig. 5). In contrast to our expectation that the application of high-pressure during the synthesis would favor the formation of a tetrahedral oxygen coordination of boron, we observe both trigonal and tetrahedral coordination in β-$Dy_2B_4O_9$. Similar observations are made in the orthoborates χ-$DyBO_3$ and χ-$ErBO_3$ synthesized under comparable conditions [6].

A classification of β-$Dy_2B_4O_9$ with the help of the "fundamental building block"-conception (FBB) after Burns et al. [37, 38] leads to the notation $2\Delta 6\square$: $\Delta\langle 3\square\rangle = \langle 4\square\rangle = \langle 3\square\rangle\Delta$. Fig. 5 shows the BO_3- and BO_4-units (encircled) which build up the fundamental building block. From our knowledge, this fundamental building block is described in this paper for the first time. This result is confirmed by Becker [36] who worked out a statistical analysis of the occurrence of different anhydrous borate fundamental building blocks and their frequency of occurrence.

The B–O bond lengths in the nearly planar BO_3-group ($\Sigma = 359.6^\circ$) vary between 136 and 140 pm (Table 4) with a mean value of 137.6 pm which is in good agreement to the average B–O distance of 137 pm [39] in planar and non-planar BO_3-units. The O–B–O angles in this BO_3-group are between 115° and 123° (Table 5). In the tetrahedral BO_4-groups of β-$Dy_2B_4O_9$, the B–O distances shift between 142 and 156 pm with an average value of 147.5 pm (Table 4) which is also consistent to the average B–O distance of 147 pm [39] in tetrahedral BO_4-units of oxoborates. The O–B–O angles in the three crystallographically independent BO_4-tetrahedra are between 101° and 123° (Table 5), whereby the upper

Table 3
Atomic coordinates and anisotropic displacement parameters (Å^2) for β-$Dy_2B_4O_9$ (space group $P\bar{1}$)

Atom	Wyckoff position	x	y	z	U_{eq}[a]
Dy1	2*i*	0.8880(1)	0.6776(1)	0.3597(1)	0.0038(1)
Dy2	2*i*	0.5474(1)	0.0912(1)	0.2851(1)	0.0035(1)
O1	2*i*	0.5038(4)	0.7889(4)	0.0200(3)	0.0043(4)
O2	2*i*	0.4206(4)	0.1835(4)	0.5554(4)	0.0045(4)
O3	2*i*	0.2356(4)	0.7353(4)	0.2109(3)	0.0039(4)
O4	2*i*	0.7796(4)	0.4067(4)	0.5233(4)	0.0045(4)
O5	2*i*	0.1374(4)	0.7156(4)	0.8574(4)	0.0048(4)
O6	2*i*	0.5397(4)	0.5387(4)	0.7483(4)	0.0045(4)
O7	2*i*	0.7733(4)	0.5717(4)	0.0409(4)	0.0037(4)
O8	2*i*	0.8126(4)	0.8691(4)	0.8817(4)	0.0054(4)
O9	2*i*	0.0668(4)	0.9541(4)	0.6764(4)	0.0059(4)
B1	2*i*	0.7326(6)	0.3356(6)	0.9812(5)	0.0032(6)
B2	2*i*	0.6616(6)	0.6813(6)	0.9268(5)	0.0036(6)
B3	2*i*	0.6259(6)	0.3581(6)	0.6516(5)	0.0037(6)
B4	2*i*	0.0049(7)	0.8537(6)	0.8121(5)	0.0047(6)

Atom	U_{11}	U_{22}	U_{33}	U_{23}	U_{13}	U_{12}
Dy1	0.0042(1)	0.0042(1)	0.0034(1)	0.0013(1)	0.0008(1)	0.0017(1)
Dy2	0.0041(1)	0.0037(1)	0.0028(1)	0.0006(1)	0.0008(1)	0.0012(1)
O1	0.004(1)	0.004(1)	0.004(1)	−0.0006(8)	0.0008(8)	0.0011(8)
O2	0.003(1)	0.005(1)	0.005(1)	0.0006(8)	−0.0005(8)	0.0010(8)
O3	0.004(1)	0.006(1)	0.003(1)	0.0020(8)	0.0008(8)	0.0027(8)
O4	0.004(1)	0.006(2)	0.004(1)	0.0019(8)	0.0020(8)	0.0018(8)
O5	0.006(2)	0.006(2)	0.004(1)	0.0019(9)	0.0011(9)	0.0042(9)
O6	0.004(2)	0.005(1)	0.005(1)	0.0001(8)	0.0002(9)	0.0028(8)
O7	0.005(2)	0.002(1)	0.004(1)	0.0006(8)	−0.0009(9)	−0.0002(8)
O8	0.004(2)	0.006(2)	0.008(2)	0.0035(9)	0.0023(9)	0.0015(9)
O9	0.006(2)	0.008(2)	0.005(1)	0.0041(9)	0.0025(9)	0.0029(9)
B1	0.004(2)	0.003(2)	0.002(2)	0.000(2)	0.000(2)	0.001(2)
B2	0.002(2)	0.004(2)	0.003(2)	0.001(2)	−0.001(2)	−0.001(2)
B3	0.003(2)	0.004(2)	0.004(2)	0.001(2)	0.001(2)	0.001(2)
B4	0.005(2)	0.005(2)	0.005(2)	0.002(2)	0.002(2)	0.003(2)

[a] U_{eq} is defined as one-third of the trace of the orthogonalized U_{ij} tensor

Table 4
Interatomic distances (pm) calculated with the single-crystal lattice parameters in β-$Dy_2B_4O_9$

Dy1–O7	230.8(3)	Dy2–O2a	226.3(3)				
Dy1–O4a	234.5(3)	Dy2–O2b	236.4(3)				
Dy1–O2	236.7(3)	Dy2–O1a	239.9(3)				
Dy1–O4b	236.7(3)	Dy2–O4	242.6(3)				
Dy1–O9a	240.2(3)	Dy2–O9	244.7(3)				
Dy1–O3	252.8(3)	Dy2–O8	249.9(3)				
Dy1–O9b	258.4(3)	Dy2–O5	254.9(3)				
Dy1–O6	263.4(3)	Dy2–O3	255.4(3)				
Dy1–O5	265.2(3)	Dy2–O1b	256.9(3)				
		Dy2–O6	260.5(3)				
B1–O7	144.2(4)	B2–O7	142.3(4)	B3–O4	146.4(5)	B4–O8	136.6(5)
B1–O3	146.1(4)	B2–O6	145.3(5)	B3–O6	146.6(5)	B4–O9	136.7(4)
B1–O1	150.1(5)	B2–O1	146.9(5)	B3–O2	148.1(5)	B4–O5	139.5(5)
B1–O5	150.2(4)	B2–O8	148.5(4)	B3–O3	155.5(5)		
	∅ = 147.7		∅ = 145.8		∅ = 149.2		∅ = 137.6

(Standard deviations in parentheses. The letters a and b indicate symmetry equivalent oxygen atoms, which coordinate to the corresponding Dy^{3+} in different interatomic distances.)

value is remarkably high. For comparison the O–B–O angles in tetragonal γ-$LiBO_2$ prepared at 1.5 GPa and 950°C do not exceed 114° [40]. Recently, we reported about two new rare-earth orthoborates χ-$DyBO_3$ and χ-$ErBO_3$ [6] synthesized under similar high-pressure conditions, wherein the BO_4-tetrahedra exhibit similar

Table 5
Interatomic angles (deg) calculated with the single-crystal lattice parameters in β-$Dy_2B_4O_9$ (standard deviations in parentheses)

O7–B1–O3	111.5(3)	O7–B2–O6	113.7(3)	O4–B3–O6	117.5(3)
O7–B1–O1	114.7(3)	O7–B2–O1	112.2(3)	O4–B3–O2	111.5(3)
O3–B1–O1	103.9(3)	O6–B2–O1	108.3(3)	O6–B3–O2	104.4(3)
O7–B1–O5	102.0(3)	O7–B2–O8	114.6(3)	O4–B3–O3	103.1(3)
O3–B1–O5	123.4(3)	O6–B2–O8	105.3(3)	O6–B3–O3	112.2(3)
O1–B1–O5	101.5(3)	O1–B2–O8	101.7(3)	O2–B3–O3	108.0(3)
	∅ = 109.5		∅ = 109.3		∅ = 109.5
O8–B4–O9	121.8(3)				
O8–B4–O5	122.9(3)				
O9–B4–O5	114.9(3)				
	∅ = 119.9				

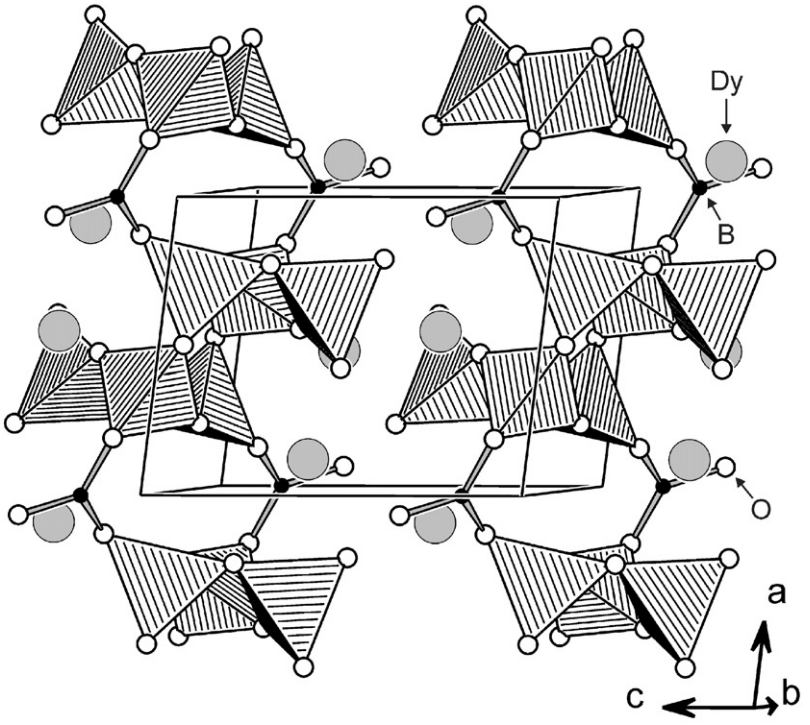

Fig. 2. Crystal structure of β-$Dy_2B_4O_9$.

distortions in the range of 102–121°. The metal ions in β-$Dy_2B_4O_9$ are coordinated by nine and 10 oxygen atoms, respectively (Fig. 6), whereby the Dy–O distances vary between 226 and 265 pm (Table 4).

For further investigations we calculated MAPLE-values (Madelung part of lattice energy) [41–43] for β-$Dy_2B_4O_9$ and compared them with the MAPLE-values of the binary components Dy_2O_3 [44] and the high-pressure modification B_2O_3-II [45]. For β-$Dy_2B_4O_9$, we received a value of 58980 kJ/mol in comparison to 59075 kJ/mol starting from the binary oxides ($1 \times Dy_2O_3$ (15199 kJ/mol) + $2 \times B_2O_3$-II (21938 kJ/mol) resulting in a deviation of 0.16%.

Also bond-valence sums were calculated for all atoms using the bond-length/bond-strength conception (ΣV) [46, 47] and the CHARDI conception (charge distribution in solids) (ΣQ) [48]. As bond-valence parameters for the bond-length/bond-strength conception, we used $R_{ij} = 137.1$ for B–O bonds and $R_{ij} = 203.6$ for Dy–O bonds [47]. Table 6 gives a comparison of the charge distribution calculated with both conceptions. The values confirm the supposed formal charges of Dy^{3+}, B^{3+}, and O^{2-}.

4.1. In situ powder diffraction

To investigate the thermal behavior of the high-pressure phase β-$Dy_2B_4O_9$, temperature-dependent measurements were performed on a STOE powder diffractometer Stadi P (Mo$K\alpha$; $\lambda = 71.073$ pm) with a computer-controlled STOE furnace. The heating element consisted of an electrically heated graphite tube

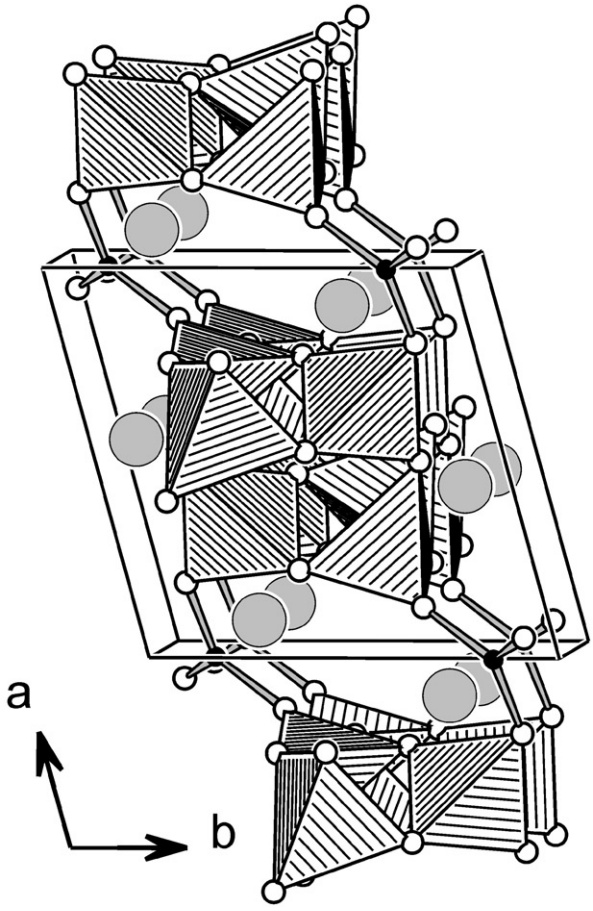

Fig. 3. Crystal structure of β-$Dy_2B_4O_9$, view along [001].

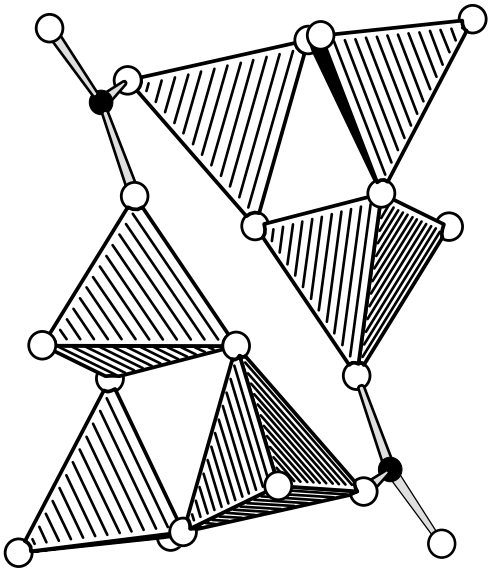

Fig. 4. Linkage of the B_3O_9-units via two trigonal BO_3-groups forming a six-membered ring.

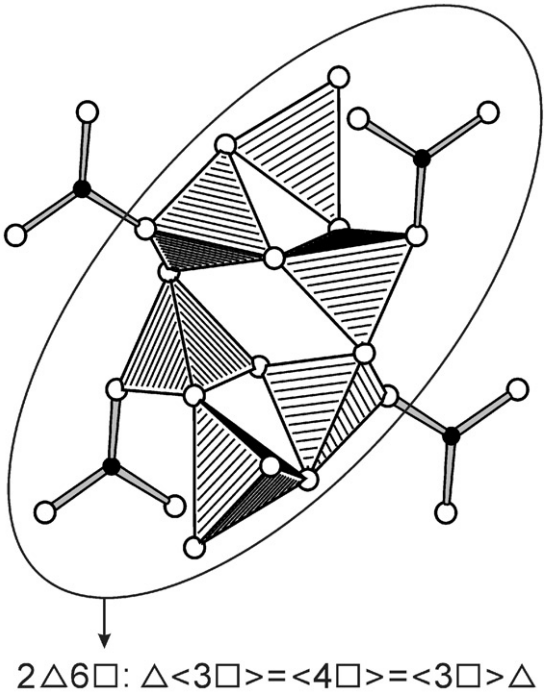

Fig. 5. Linkage of the B_3O_9-units forming a four-membered ring. The encircled area represents the fundamental building block of β-$Dy_2B_4O_9$.

holding the sample capillary vertically with respect to the scattering plane. Bores in the graphite tube permitted unobstructed pathways for the primary beam as well as for the scattered radiation. The temperature measured by a thermocouple in the graphite tube was kept constant to within 0.2°C. The heating rate between different temperatures was set to 22°C/min. For temperature stabilization, a time of 3 min was given before start of each data acquisition. Successive heating of the high-pressure phase β-$Dy_2B_4O_9$ (Fig. 7) led in the range of 700–800°C to a decomposition into the normal pressure modifications π-$DyBO_3$, μ-$DyBO_3$ [49] and molten B_2O_3. Further heating showed the complete transformation of π-$DyBO_3$ into the high-temperature modification μ-$DyBO_3$ above 900°C. Subsequent cooling resulted in a retransformation to the room temperature modification π-$DyBO_3$ below 700°C.

4.2. Infrared absorption spectroscopy

The infrared (IR) spectrum of β-$Dy_2B_4O_9$ (Fig. 8) was recorded on a Bruker IFS 66v/S spectrometer scanning a range from 400 to 4000 cm^{-1}. The sample was thoroughly mixed with dried KBr (5 mg sample, 500 mg KBr) in a glove box under dried argon atmosphere.

Fig. 8 shows the section 400–2800 cm^{-1} of the infrared spectrum. The absorption peaks between 790 and 1200 cm^{-1} are those typical for the tetrahedral borate group BO_4 as in YBO_3, $GdBO_3$, or $TaBO_4$ [50–52]. The typical absorptions of the triangular BO_3-group appear between 1450 and 1200 cm^{-1} and below 790 cm^{-1} as in $LaBO_3$ [53, 54] or EuB_2O_4 [55]. Due to

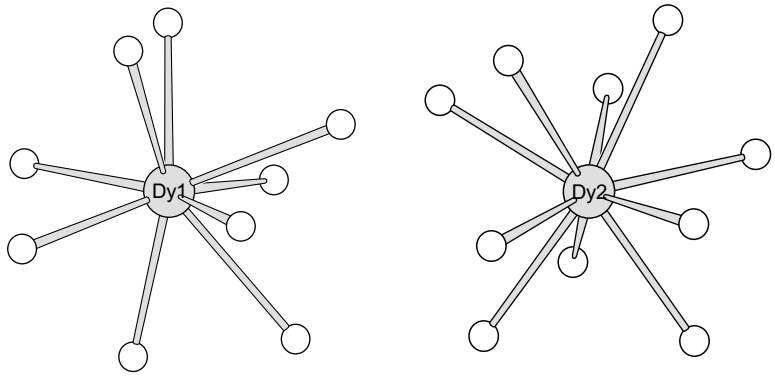

Fig. 6. Coordination spheres of Dy^{3+} (gray spheres) in the crystal structure of β-$Dy_2B_4O_9$.

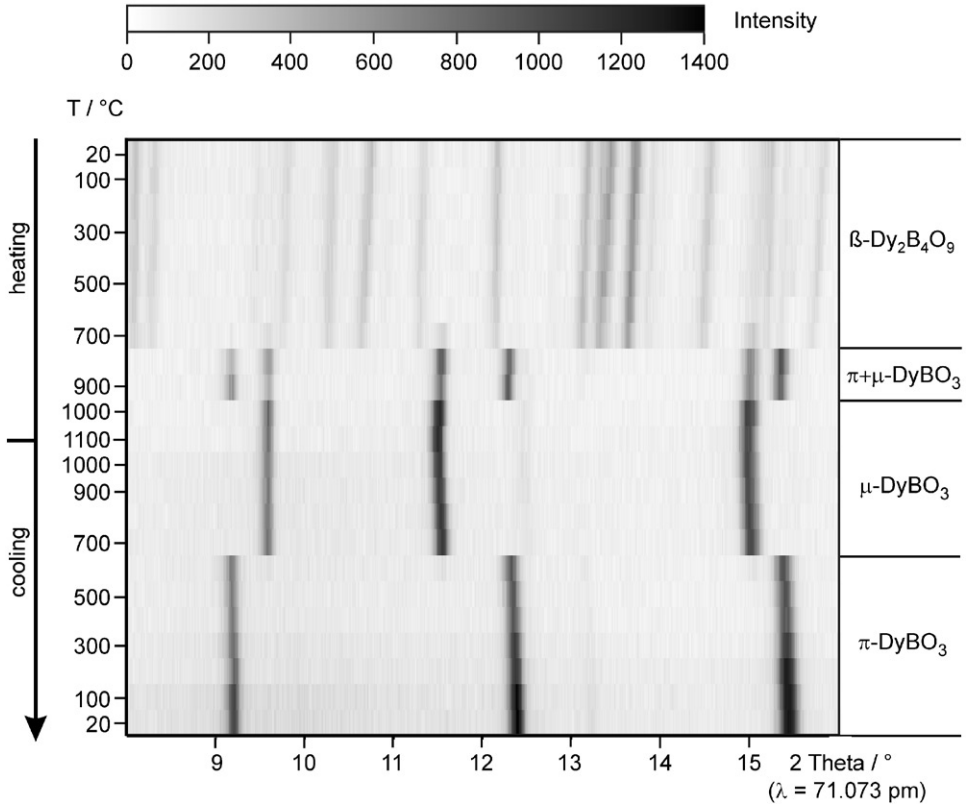

Fig. 7. Temperature-dependent X-ray thermodiffractometric powder patterns of the decomposition of β-$Dy_2B_4O_9$.

Table 6
Charge distribution in β-$Dy_2B_4O_9$ calculated with the bond-length/bond-strength conception (ΣV) [46,47] and the CHARDI conception (ΣQ) [48]

	Dy1	Dy2	B1	B2	B3	B4	O1	O2	O3	O4	O5	O6	O7	O8	O9
ΣV	2.98	3.24	3.01	3.17	2.90	2.96	−2.08	−2.11	−1.90	−1.97	−2.08	−1.99	−2.17	−2.04	−1.94
ΣQ	2.97	3.01	3.00	2.96	3.03	3.03	−1.96	−2.05	−1.85	−2.02	−2.00	−1.97	−2.19	−1.98	−1.97

the combination of one BO_3- and three crystallographic independent BO_4-units in the solid state, a detailed assignment of the vibrations is difficult. Although the sample consists mainly of crystalline parts (β-$Dy_2B_4O_9$) we can not exclude the appearance of additional weak vibrations by the flux impurities. In the upper range (4000–2800 cm^{-1}) no absorption bands due to hydrogen (OH) were detectable.

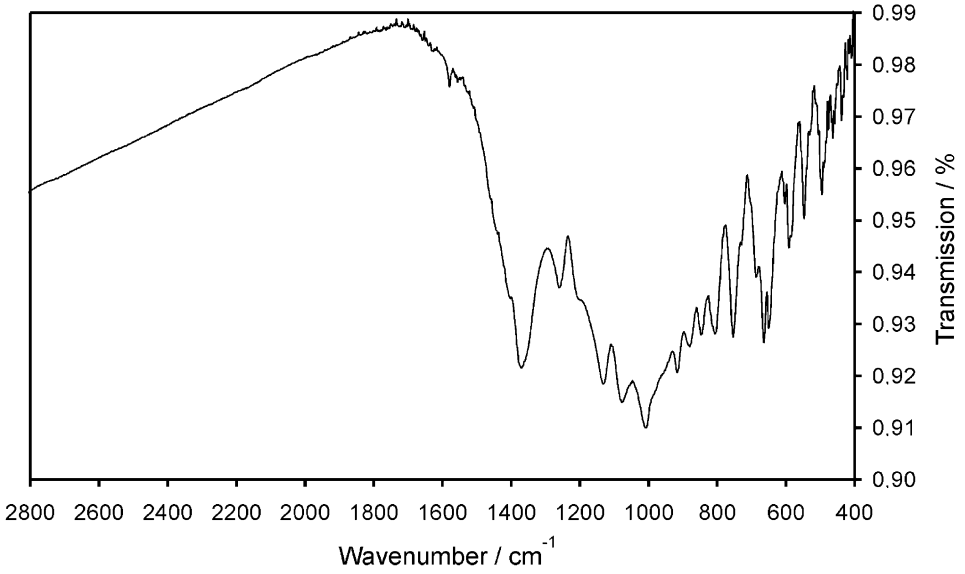

Fig. 8. Infrared spectrum of β-$Dy_2B_4O_9$.

5. Conclusion

In this paper, we described the synthesis of the new rare-earth oxoborate β-$Dy_2B_4O_9$ via multianvil high-pressure synthesis from Dy_2O_3 and boron oxide B_2O_3 in a flux of B_2O_3/Na_2O_2. β-$Dy_2B_4O_9$ exhibits a new structure type with bands of linked BO_3- and BO_4-tetrahedra which can be described with the new fundamental building block $2\Delta 6\square{:}\Delta\langle 3\square\rangle = \langle 4\square\rangle = \langle 3\square\rangle\Delta$. In contrast to the synthesis of α-$Dy_2B_4O_9$ (without flux) the presence of a B_2O_3/Na_2O_2 flux leads to the formation of a new polymorph. Although the synthesis takes place under extreme high-pressure/high-temperature conditions, where corner- and edge-sharing of BO_4-tetrahedra is observed in the case of α-$Dy_2B_4O_9$, we find only corner-sharing of BO_3- and BO_4-units in the presented β-$Dy_2B_4O_9$.

Acknowledgments

We thank Prof. Dr. W. Schnick, Department Chemie of the University of Munich (LMU), for his steady interest and continuous support of this work. Special thanks go to Dr. H. Piotrowski for collecting the single crystal data and Dipl. Chem. S. Correll for the in situ powder diffraction measurements.

References

[1] P. Becker, Adv. Mater. 10 (1998) 979.
[2] T. Sasaki, Y. Mori, M. Yoshimura, Y.K. Yap, T. Kamimura, Mater. Sci. Eng. 30 (2000) 1.
[3] D.A. Keszler, Curr. Opin. Solid State Mater. Sci. 1 (1996) 204.
[4] J. Weidelt, Z. Anorg. Allg. Chem. 374 (1970) 26.
[5] H. Bergmann (Ed.), Gmelin Handbook of Inorganic and Organometallic Chemistry, C11b, 8th Edition, Springer, Berlin, 1991.
[6] H. Huppertz, B. von der Eltz, J. Solid State Chem. 166 (2002) 203.
[7] E.M. Levin, C.R. Robbins, J.L. Warring, J. Am. Ceram. Soc. 44 (1961) 87.
[8] S.F. Bartram, Proceedings of the Third Conference Rare Earth Research, Clearwater, FL, 1964, p. 165.
[9] J.H. Lin, M.Z. Su, K. Wurst, E. Schweda, J. Solid State Chem. 126 (1996) 287.
[10] J.H. Lin, S. Zhou, L.Q. Yang, G.Q. Yao, M.Z. Su, J. Solid State Chem. 134 (1997) 158.
[11] J.H. Lin, L.P. You, G.X. Lu, L.Q. Yang, M.Z. Su, J. Mater. Chem. 8 (1998) 1051.
[12] G. Canneri, Gazz. Chim. Ital. 56 (1926) 450.
[13] I.V. Tananaev, B.F. Dzhurinskii, I.M. Belyakov, Izv. Akad. Nauk SSSR Neorgan. Mater. 2 (1966) 1791.
[14] H.U. Bambauer, J. Weidelt, J.St. Ysker, Z. Kristallogr. 130 (1969) 207.
[15] I.V. Tananaev, B.F. Dzhurinskii, B.F. Chistova, Izv. Akad. Nauk SSSR Neorgan. Mater. 11 (1975) 165.
[16] C. Sieke, T. Nikelski, T. Schleid, Z. Anorg. Allg. Chem. 628 (2002) 819.
[17] H. Huppertz, B. von der Eltz, J. Am. Chem. Soc. 124 (2002) 9376.
[18] H. Huppertz, unpublished results.
[19] H. Emme, H. Huppertz, Z. Anorg. Allg. Chem. 628 (2002) 2165.
[20] H. Huppertz, Z. Naturforsch. 56b (2001) 697.
[21] D. Walker, M.A. Carpenter, C.M. Hitch, Am. Mineral. 75 (1990) 1020.
[22] D. Walker, Am. Mineral. 76 (1991) 1092.
[23] D.C. Rubie, Phase Trans. 68 (1999) 431.
[24] M. Marezio, H.A. Plettinger, W.H. Zachariasen, Acta Crystallogr. 16 (1963) 594.
[25] H. König, R. Hoppe, M. Jansen, Z. Anorg. Allg. Chem. 449 (1979) 91.
[26] H. König, R. Hoppe, Z. Anorg. Allg. Chem. 434 (1977) 232.
[27] J. Krogh-Moe, Acta Crystallogr. B 30 (1974) 747.
[28] J. Krogh-Moe, Acta Crystallogr. B 28 (1972) 1571.

[29] A. Hymann, A. Perloff, F. Mauer, S. Block, Acta Crystallogr. B 22 (1967) 815.
[30] J. Mascetti, M. Vlasse, C. Fouassier, J. Solid State Chem. 39 (1981) 228.
[31] Y. Zhang, X.L. Chen, J.K. Liang, T. Xu, J. Alloys Comp. 333 (2002) 72.
[32] J.W. Visser, J. Appl. Crystallogr. 2 (1969) 89.
[33] W. Herrendorf, H. Bärnighausen, HABITUS, Program for Numerical Absorption Correction, University of Karlsruhe/Gießen, Germany, 1993/1997.
[34] G. M. Sheldrick, SHELXS-97, Program for the Solution of Crystal Structures, University of Göttingen, Germany, 1997.
[35] G. M. Sheldrick, SHELXL-97, Program for Crystal Structure Refinement, University of Göttingen, Germany, 1997.
[36] P. Becker, Z. Kristallogr. 216 (2001) 523.
[37] P.C. Burns, J.D. Grice, F.C. Hawthorne, Can. Mineral. 33 (1995) 1131.
[38] J.D. Grice, P.C. Burns, F.C. Hawthorne, Can. Mineral. 37 (1999) 731.
[39] F.C. Hawthorne, P.C. Burns, J.D. Grice, in: E.S. Grew, L.M. Anovitz (Eds.), Boron: Mineralogy, Petrology, and Geochemistry, Reviews in Mineralogy 33, Mineralogical Society of America, Washington, DC, 1996.
[40] M. Marezio, J.P. Remeika, J. Chem. Phys. 44 (1966) 3348.
[41] R. Hoppe, Angew. Chem. 78 (1966) 52;
R. Hoppe, Angew. Chem. Int. Ed. Engl. 5 (1966) 95.
[42] R. Hoppe, Angew. Chem. 82 (1970) 7;
R. Hoppe, Angew. Chem. Int. Ed. Engl. 9 (1970) 25.
[43] R. Hoppe, R. Hübenthal, MAPLE, Program for the Calculation of MAPLE-Values, Vers. 4, University of Gießen, 1993.
[44] W. Hase, Phys. Status Solidi 3 (1963) 446.
[45] C.T. Prewitt, R.D. Shannon, Acta Crystallogr. B 24 (1968) 869.
[46] I.D. Brown, D. Altermatt, Acta Crystallogr. B 41 (1985) 244.
[47] N.E. Brese, M. O'Keeffe, Acta crystallogr. B 47 (1985) 192.
[48] R. Hoppe, S. Voigt, H. Glaum, J. Kissel, H.P. Müller, K. Bernet, J. Less-Common Met. 156 (1989) 105.
[49] E.M. Levin, R.S. Roth, J.B. Martin, Am. Mineral. 46 (1961) 1030.
[50] M. Ren, J.H. Lin, Y. Dong, L.Q. Yang, M.Z. Su, L.P. You, Chem. Mater. 11 (1999) 1576.
[51] J.P. Laperches, P. Tarte, Spectrochim. Acta 22 (1966) 1201.
[52] G. Blasse, G.P.M. van den Heuvel, Phys. Stat. Sol. 19 (1973) 111.
[53] W.C. Steele, J.C. Decius, J. Chem. Phys. 25 (1956) 1184.
[54] R. Böhlhoff, H.U. Bambauer, W. Hoffmann, Z. Kristallogr. 133 (1971) 386.
[55] K. Machida, H. Hata, K. Okuno, G. Adachi, J. Shiokawa, J. Inorg. Nucl. Chem. 41 (1979) 1425.